Title
A comparison of Doppler optical coherence tomography methods

Journal
Biomedical Optics Express, 3(10)

ISSN
2156-7085

Authors
Liu, Gangjun
Lin, Alexander J.
Tromberg, Bruce J.
et al.

Publication Date
2012-09-26

Peer reviewed

Biomedical Optics EXPRESS

A comparison of Doppler optical coherence tomography methods

Gangjun Liu,[1,2,*] Alexander J. Lin,[1,2] Bruce J. Tromberg,[1,2] and Zhongping Chen[1,2,3]

[1]*Beckman Laser Institute, University of California, Irvine, Irvine, CA 92617, USA*
[2]*Department of Biomedical Engineering, University of California, Irvine, Irvine, CA 92617, USA*
[3]*z2chen@uci.edu*
**gangjun@gmail.com*

Abstract: We compare, in detail, the phase-resolved color Doppler (PRCD), phase-resolved Doppler variance (PRDV) and intensity-based Doppler variance (IBDV) methods. All the methods are able to quantify flow speed when the flow rate is within a certain range, which is dependent on the adjacent A-line time interval. While PRCD is most sensitive when the flow direction is along the probing beam, PRDV and IBDV can be used to measure the flow when the flow direction is near perpendicular to the probing beam. However, the values of PRDV and IBDV are Doppler angle-dependent when the Doppler angle is above a certain threshold. The sensitivity of all the methods can be improved by increasing the adjacent A-line time interval while still maintaining a high sampling density level. We also demonstrate for the first time, to the best of our knowledge, high resolution inter-frame PRDV method. In applications where mapping vascular network such as angiogram is more important than flow velocity quantification, IBDV and PRDV images show better contrast than PRCD images. The IBDV and PRDV show very similar characteristics and demonstrate comparable results for vasculature mapping. However, the IBDV is less sensitive to bulk motion and with less post-processing steps, which is preferred for fast data processing situations. *In vivo* imaging of mouse brain with intact skull and human skin with the three methods were demonstrated and the results were compared. The IBDV method was found to be able to obtain high resolution image with a relative simple processing procedure.

OCIS codes: (170.3890) Medical optics instrumentation; (170.4500) Optical coherence tomography.

References and links

1. D. Huang, E. A. Swanson, C. P. Lin, J. S. Schuman, W. G. Stinson, W. Chang, M. R. Hee, T. Flotte, K. Gregory, C. A. Puliafito, and J. G. Fujimoto, "Optical coherence tomography," Science **254**(5035), 1178–1181 (1991).
2. J. F. de Boer, B. Cense, B. H. Park, M. C. Pierce, G. J. Tearney, and B. E. Bouma, "Improved signal-to-noise ratio in spectral-domain compared with time-domain optical coherence tomography," Opt. Lett. **28**(21), 2067–2069 (2003).
3. M. A. Choma, M. V. Sarunic, C. Yang, and J. A. Izatt, "Sensitivity advantage of swept source and Fourier domain optical coherence tomography," Opt. Express **11**(18), 2183–2189 (2003).
4. R. Leitgeb, C. K. Hitzenberger, and A. F. Fercher, "Performance of fourier domain vs. time domain optical coherence tomography," Opt. Express **11**(8), 889–894 (2003).
5. Z. Chen, T. E. Milner, S. Srinivas, X. J. Wang, A. Malekafzali, M. J. C. van Gemert, and J. S. Nelson, "Noninvasive imaging of *in vivo* blood flow velocity using optical Doppler tomography," Opt. Lett. **22**(14), 1119–1121 (1997).
6. J. A. Izatt, M. D. Kulkarni, S. Yazdanfar, J. K. Barton, and A. J. Welch, "*In vivo* bidirectional color Doppler flow imaging of picoliter blood volumes using optical coherence tomography," Opt. Lett. **22**(18), 1439–1441 (1997).
7. Z. Chen, T. E. Milner, X. Wang, S. Srinivas, and J. S. Nelson, "Optical Doppler tomography: imaging *in vivo* blood flow dynamics following pharmacological intervention and photodynamic therapy," Photochem. Photobiol. **67**(1), 56–60 (1998).

#172899 - $15.00 USD Received 19 Jul 2012; revised 11 Sep 2012; accepted 19 Sep 2012; published 26 Sep 2012

8. Y. Zhao, Z. Chen, C. Saxer, S. Xiang, J. F. de Boer, and J. S. Nelson, "Phase-resolved optical coherence tomography and optical Doppler tomography for imaging blood flow in human skin with fast scanning speed and high velocity sensitivity," Opt. Lett. **25**(2), 114–116 (2000).
9. Y. Zhao, K. M. Brecke, H. Ren, Z. Ding, J. S. Nelson, and Z. Chen, "Three-dimensional reconstruction of *in vivo* blood vessels in human skin using phase-resolved optical Doppler tomography," IEEE J. Sel. Top. Quantum Electron. **7**(6), 931–935 (2001).
10. S. Makita, Y. Hong, M. Yamanari, T. Yatagai, and Y. Yasuno, "Optical coherence angiography," Opt. Express **14**(17), 7821–7840 (2006).
11. D. Y. Kim, J. Fingler, J. S. Werner, D. M. Schwartz, S. E. Fraser, and R. J. Zawadzki, "*In vivo* volumetric imaging of human retinal circulation with phase-variance optical coherence tomography," Biomed. Opt. Express **2**(6), 1504–1513 (2011).
12. J. Fingler, R. J. Zawadzki, J. S. Werner, D. Schwartz, and S. E. Fraser, "Volumetric microvascular imaging of human retina using optical coherence tomography with a novel motion contrast technique," Opt. Express **17**(24), 22190–22200 (2009).
13. H. Ren, Y. Wang, J. S. Nelson, and Z. Chen, "Power optical Doppler tomography imaging of blood vessel in human skin and M-mode Doppler imaging of blood flow in chick chrioallantoic membrane," Proc. SPIE **4956**, 225–231 (2003).
14. J. Barton and S. Stromski, "Flow measurement without phase information in optical coherence tomography images," Opt. Express **13**(14), 5234–5239 (2005).
15. A. Mariampillai, M. K. Leung, M. Jarvi, B. A. Standish, K. Lee, B. C. Wilson, A. Vitkin, and V. X. Yang, "Optimized speckle variance OCT imaging of microvasculature," Opt. Lett. **35**(8), 1257–1259 (2010).
16. A. Mariampillai, B. A. Standish, E. H. Moriyama, M. Khurana, N. R. Munce, M. K. Leung, J. Jiang, A. Cable, B. C. Wilson, I. A. Vitkin, and V. X. Yang, "Speckle variance detection of microvasculature using swept-source optical coherence tomography," Opt. Lett. **33**(13), 1530–1532 (2008).
17. R. Motaghiannezam and S. Fraser, "Logarithmic intensity and speckle-based motion contrast methods for human retinal vasculature visualization using swept source optical coherence tomography," Biomed. Opt. Express **3**(3), 503–521 (2012).
18. Y. Yasuno, Y. Hong, S. Makita, M. Yamanari, M. Akiba, M. Miura, and T. Yatagai, "*In vivo* high-contrast imaging of deep posterior eye by 1-μm swept source optical coherence tomography and scattering optical coherence angiography," Opt. Express **15**(10), 6121–6139 (2007).
19. E. Jonathan, J. Enfield, and M. J. Leahy, "Correlation mapping method for generating microcirculation morphology from optical coherence tomography (OCT) intensity images," J Biophotonics **4**(9), 583–587 (2011).
20. Y. Jia, O. Tan, J. Tokayer, B. Potsaid, Y. Wang, J. J. Liu, M. F. Kraus, H. Subhash, J. G. Fujimoto, J. Hornegger, and D. Huang, "Split-spectrum amplitude-decorrelation angiography with optical coherence tomography," Opt. Express **20**(4), 4710–4725 (2012).
21. G. Liu, L. Chou, W. Jia, W. Qi, B. Choi, and Z. Chen, "Intensity-based modified Doppler variance algorithm: application to phase instable and phase stable optical coherence tomography systems," Opt. Express **19**(12), 11429–11440 (2011).
22. Y. Zhao, Z. Chen, C. Saxer, Q. Shen, S. Xiang, J. F. de Boer, and J. S. Nelson, "Doppler standard deviation imaging for clinical monitoring of *in vivo* human skin blood flow," Opt. Lett. **25**(18), 1358–1360 (2000).
23. H. Ren, T. Sun, D. J. MacDonald, M. J. Cobb, and X. Li, "Real-time *in vivo* blood-flow imaging by moving-scatterer-sensitive spectral-domain optical Doppler tomography," Opt. Lett. **31**(7), 927–929 (2006).
24. H. Ren and X. Li, "Clutter rejection filters for optical Doppler tomography," Opt. Express **14**(13), 6103–6112 (2006).
25. R. K. Wang, S. L. Jacques, Z. Ma, S. Hurst, S. R. Hanson, and A. Gruber, "Three dimensional optical angiography," Opt. Express **15**(7), 4083–4097 (2007).
26. Z. Yuan, Z. C. Luo, H. G. Ren, C. W. Du, and Y. Pan, "A digital frequency ramping method for enhancing Doppler flow imaging in Fourier-domain optical coherence tomography," Opt. Express **17**(5), 3951–3963 (2009).
27. Y. K. Tao, A. M. Davis, and J. A. Izatt, "Single-pass volumetric bidirectional blood flow imaging spectral domain optical coherence tomography using a modified Hilbert transform," Opt. Express **16**(16), 12350–12361 (2008).
28. S. Zotter, M. Pircher, T. Torzicky, M. Bonesi, E. Götzinger, R. A. Leitgeb, and C. K. Hitzenberger, "Visualization of microvasculature by dual-beam phase-resolved Doppler optical coherence tomography," Opt. Express **19**(2), 1217–1227 (2011).
29. S. Makita, F. Jaillon, M. Yamanari, M. Miura, and Y. Yasuno, "Comprehensive *in vivo* micro-vascular imaging of the human eye by dual-beam-scan Doppler optical coherence angiography," Opt. Express **19**(2), 1271–1283 (2011).
30. L. An, J. Qin, and R. K. Wang, "Ultrahigh sensitive optical microangiography for *in vivo* imaging of microcirculations within human skin tissue beds," Opt. Express **18**(8), 8220–8228 (2010).
31. G. Liu, W. Jia, V. Sun, B. Choi, and Z. Chen, "High-resolution imaging of microvasculature in human skin in-vivo with optical coherence tomography," Opt. Express **20**(7), 7694–7705 (2012).
32. H. Ren, K. M. Brecke, Z. Ding, Y. Zhao, J. S. Nelson, and Z. Chen, "Imaging and quantifying transverse flow velocity with the Doppler bandwidth in a phase-resolved functional optical coherence tomography," Opt. Lett. **27**(6), 409–411 (2002).

#172899 - $15.00 USD Received 19 Jul 2012; revised 11 Sep 2012; accepted 19 Sep 2012; published 26 Sep 2012

33. V. Yang, M. Gordon, B. Qi, J. Pekar, S. Lo, E. Seng-Yue, A. Mok, B. Wilson, and I. Vitkin, "High speed, wide velocity dynamic range Doppler optical coherence tomography (Part I): System design, signal processing, and performance," Opt. Express **11**(7), 794–809 (2003).
34. B. Rao, L. Yu, H. K. Chiang, L. C. Zacharias, R. M. Kurtz, B. D. Kuppermann, and Z. Chen, "Imaging pulsatile retinal blood flow in human eye," J. Biomed. Opt. **13**(4), 040505 (2008).
35. L. Yu, E. Nguyen, G. Liu, B. Choi, and Z. Chen, "Spectral Doppler optical coherence tomography imaging of localized ischemic stroke in a mouse model," J. Biomed. Opt. **15**(6), 066006 (2010).
36. Y.-C. Ahn, W. Jung, and Z. Chen, "Quantification of a three-dimensional velocity vector using spectral-domain Doppler optical coherence tomography," Opt. Lett. **32**(11), 1587–1589 (2007).
37. Y.-C. Ahn, W. Jung, and Z. Chen, "Optical sectioning for microfluidics: secondary flow and mixing in a meandering microchannel," Lab Chip **8**(1), 125–133 (2008).
38. H. C. Hendargo, R. P. McNabb, A.-H. Dhalla, N. Shepherd, and J. A. Izatt, "Doppler velocity detection limitations in spectrometer-based versus swept-source optical coherence tomography," Biomed. Opt. Express **2**(8), 2175–2188 (2011).
39. G. Liu, W. Qi, L. Yu, and Z. Chen, "Real-time bulk-motion-correction free Doppler variance optical coherence tomography for choroidal capillary vasculature imaging," Opt. Express **19**(4), 3657–3666 (2011).
40. L. Yu and Z. Chen, "Doppler variance imaging for three-dimensional retina and choroid angiography," J. Biomed. Opt. **15**(1), 016029 (2010).

1. Introduction

Optical coherence tomography (OCT) is a non-invasive, high resolution imaging modality capable of capturing three-dimensional images from highly scattering biological tissue [1]. In the past few years, due to the development of fast swept laser sources and high speed detector arrays, Fourier domain OCT systems have experienced dramatic improvement compared with the time domain OCT systems, in terms of imaging speed and sensitivity [2–4]. The functional extension of the OCT technique to provide information beyond the tissue structure has numerous applications in biomedical imaging. One important division of functional OCT is the mapping of vascular network and extraction of blood vessel information such as blood flow speed and blood flow direction.

OCT is analogous to ultrasound tomography, but uses light waves instead of sound waves. Analogous to Doppler ultrasound, Doppler OCT (D-OCT) or optical Doppler tomography (ODT) is a functional extension of OCT which combines the Doppler principle with OCT [5–7]. Phase-resolved D-OCT is one of the preferred D-OCT methods to extract the Doppler frequency because of its high velocity sensitivity [8,9]. The phase-resolved color Doppler (PRCD) uses the phase difference among the adjacent A-lines to extract the Doppler frequency shift and quantitative information such as blood flow velocity and blood flow direction can be obtained. Several extensions of phase-resolved methods has been reported. One uses the absolute value of the phase difference [10]. Another adopts the variance of several adjacent A-line phase differences [11,12]. The physical principle behind the phase-resolved methods is the Doppler effect.

There are considerable interests in imaging blood vessels using intensity or amplitude information instead of phase information. Ren et al., for the first time, demonstrated a power Doppler angiography method by using band-pass filtered intensity image for imaging the moving scatterer in tissue [13]. Barton et al. proposed a method based on the speckle of conventional amplitude optical coherence tomography images [14]. Mariampillai et al. used the speckle variance in a small 3D volume to image blood vessels [15,16]. Recently, the logarithmic intensity variance and differential logarithmic intensity variance are proposed by Motaghiannezam et al. [17]. Yasuno et al. used the intensity threshold binarization-based method for retinal and choroidal blood vessel imaging [18]. Jonathan et al. used a two-dimensional correlation map based on the OCT intensity images for blood vessel extraction [19]. Jia et al. developed a split-spectrum amplitude-decorrelation angiography method [20]. Recently, we proposed an intensity-based method that used an algorithm derived from a modified Doppler variance algorithm [21]. The physical principle behind the intensity-resolved methods is the speckle effect.

#172899 - $15.00 USD Received 19 Jul 2012; revised 11 Sep 2012; accepted 19 Sep 2012; published 26 Sep 2012

In addition to the methods which are purely based on phase or intensity information, there are other phase resolved methods which used both the phase and intensity information. One of such methods is the phase-resolved Doppler variance (PRDV) method [22]. Doppler variance uses the autocorrelation algorithm which involves the complex OCT data at each location. Another group of such methods involves operations such as filtering on the original acquired fringes [23–27]. Methods that fall in this group include moving-scatterer-sensitive optical Doppler tomography, optical microangiography, a digital frequency ramping method and single-pass volumetric bidirectional blood flow imaging method [23–27].

For the phase-resolved ODT method, the velocity sensitivity can be improved by increasing the time interval between adjacent A-lines used in the algorithm. This has been implemented in Doppler OCT systems [13,28–30]. As pointed out in our recent publications, sensitivity of intensity-based Doppler variance (IBDV) method can also be improved by increasing the time interval between adjacent A-lines used in the algorithm [31]. For methods involving both intensity and phase information, the sensitivity has also been improved by applying the algorithm along the slow scanning direction, which increases the time interval accordingly [30].

In this paper, we will compare, in detail, three methods which are using, respectively, phase information (PRCD), intensity information (IBDV) and both phase and intensity information (PRDV). Flow phantoms are used to obtain the characteristics of these methods. These characteristics include flow velocity determination, incident angle dependence, and sensitivity improvement by increasing the adjacent A-line time intervals. It was found that all the methods are able to quantify the flow speed when the flow rate is within a certain range, which is dependent on the adjacent A-line time interval. While PRCD is most sensitive when the flow direction is along the probing beam, PRDV and IBDV can be used to measure the flow when the flow direction is near perpendicular to the probing beam. The PRDV and IBDV are not sensitive to the Doppler angle when the angle is less than 12 degrees. However, the PRDV and IBDV are Doppler angle-dependent when the Doppler angle is larger than 12 degrees. The sensitivity of all the methods can be improved by increasing the adjacent A-line time interval while still maintaining a high sampling density level. *In vivo* imaging of mouse brain with intact skull and human palm skin are demonstrated. The microvascular network images obtained with the three methods are compared.

2. The methods

PRCD OCT uses the adjacent A-line phase difference to extract the average Doppler frequency:

$$\overline{f} = \frac{d\theta(z)}{dt} = \frac{\theta_{j+1,z} - \theta_{j,z}}{T}, \tag{1}$$

where $\overline{f}$ is Doppler frequency, and are the phases for the signal at the depth z of the $(j + 1)$th and jth A-line, and T is the time interval between adjacent A-lines. It has become one of the preferred methods for Doppler OCT due to its high velocity sensitivity. Using the autocorrelation algorithm, Eq. (1) can be rewritten as [9]

$$\overline{f} = \frac{1}{T}\arctan\left[\frac{\mathrm{Im}(A_{j+1,z})\,\mathrm{Re}(A_{j,z}) - \mathrm{Im}(A_{j,z})\,\mathrm{Re}(A_{j+1,z})}{\mathrm{Re}(A_{j,z})\,\mathrm{Re}(A_{j+1,z}) + \mathrm{Im}(A_{j+1,z})\,\mathrm{Im}(A_{j,z})}\right], \tag{2}$$

where $\mathrm{Re}(A_j)$ and $\mathrm{Re}(A_{jz})$ are, respectively, the real and imaginary part of the complex data A_{jz}. The algorithm shown in Eq. (2) uses only the phase information and is purely phase-based.

PRDV is an extension of the phase-resolved D-OCT technique. It uses the variance of the Doppler frequency spectrum to map the flow. Doppler variance has the benefits of less sensitivity to the pulsatile nature of blood flow, less sensitivity to the incident angle, and it

#172899 - $15.00 USD Received 19 Jul 2012; revised 11 Sep 2012; accepted 19 Sep 2012; published 26 Sep 2012

may be used to obtain the transverse flow velocity [22,32]. Let σ denote the standard deviation of the Doppler spectrum; the Doppler variance σ^2 can be obtained [22]:

$$\sigma^2 = \frac{\int (f-\overline{f})^2 P(f) df}{\int P(f) df} = \overline{f^2} - \overline{f}^2. \tag{3}$$

With the help of autocorrelation technology, the variance can be expressed as [22]

$$\sigma^2 = \frac{1}{T^2}\left(1 - \frac{\left|A_{j,z}A_{j+1,z}^*\right|}{\frac{1}{2}\left(A_{j,z}A_{j,z}^* + A_{j+1,z}A_{j+1,z}^*\right)}\right). \tag{4}$$

Usually, the equations are used together with averaging to improve signal to noise ratio (SNR). Averaging can be done in the lateral direction (temporal direction) so that Eqs. (2) and (4) become:

$$\overline{f} = \frac{1}{T}\arctan\left\{\frac{\sum_{j=1}^{J}\left[\mathrm{Im}(A_{j+1,z})\,\mathrm{Re}(A_{j,z}) - \mathrm{Im}(A_{j,z})\,\mathrm{Re}(A_{j+1,z})\right]}{\sum_{j=1}^{J}\left[\mathrm{Re}(A_{j,z})\,\mathrm{Re}(A_{j+1,z}) + \mathrm{Im}(A_{j+1,z})\,\mathrm{Im}(A_{j,z})\right]}\right\}, \tag{5}$$

$$\sigma^2 = \frac{1}{T^2}\left[1 - \frac{\left|\sum_{j=1}^{J}\left(A_{j,z}A_{j+1,z}^*\right)\right|}{\sum_{j=1}^{J}\frac{1}{2}\left(A_{j,z}A_{j,z}^* + A_{j+1,z}A_{j+1,z}^*\right)}\right], \tag{6}$$

where J is the number of A-lines that are averaged. The averaging could be also performed in both lateral and depth direction, and Eqs. (5) and (6) become [33]

$$\overline{f} = \frac{1}{T}\arctan\left\{\frac{\sum_{j=1}^{J}\sum_{z=1}^{N}\left[\mathrm{Im}(A_{j+1,z})\,\mathrm{Re}(A_{j,z}) - \mathrm{Im}(A_{j,z})\,\mathrm{Re}(A_{j+1,z})\right]}{\sum_{j=1}^{J}\sum_{z=1}^{N}\left[\mathrm{Re}(A_{j,z})\,\mathrm{Re}(A_{j+1,z}) + \mathrm{Im}(A_{j+1,z})\,\mathrm{Im}(A_{j,z})\right]}\right\}, \tag{7}$$

$$\sigma^2 = \frac{1}{T^2}\left[1 - \frac{\left|\sum_{j=1}^{J}\sum_{z=1}^{N}\left(A_{j,z}A_{j+1,z}^*\right)\right|}{\sum_{j=1}^{J}\sum_{z=1}^{N}\frac{1}{2}\left(A_{j,z}A_{j,z}^* + A_{j+1,z}A_{j+1,z}^*\right)}\right] \tag{8}$$

where J is the number of A-lines that are averaged and N is the number of depth points that are averaged. Compared with lateral averaging only algorithms as Eqs. (5) and (6), averaging along both lateral and depth direction as Eqs. (7) and (8) can reduce the background noise and improve the image quality. The choosing of J and N are dependent on application. Generally, a larger J and N will increase SNR, increase the computing time and decrease resolution. In this manuscript, we will adopt Eqs. (7) and (8) for the calculation of PRCD and PRDV and $J = 4$, $N = 4$ to balance the SNR and resolution.

It should be noted that the variance value in Eqs. (6) and (8) is related to the complex OCT value, which is a function of both the intensity and phase values. Recently, we have proposed

#172899 - $15.00 USD Received 19 Jul 2012; revised 11 Sep 2012; accepted 19 Sep 2012; published 26 Sep 2012

the IBDV method which is based on the modified Doppler variance algorithm of Eq. (8) [21,31]:

$$\sigma^2 = \frac{1}{T^2}\left[1 - \frac{\sum_{j=1}^{J}\sum_{z=1}^{N}\left(\left|A_{j,z}\right|\left|A_{j+1,z}\right|\right)}{\sum_{j=1}^{J}\sum_{z=1}^{N}\frac{1}{2}\left(\left|A_{j,z}\right|^2 + \left|A_{j+1,z}\right|^2\right)}\right]. \quad (9)$$

The modified algorithm uses only the intensity information, and it is suitable for phase instable OCT systems. In the following, Eq. (9) with J = 4, N = 4 will be used for the calculation of IBDV, and the final variance value obtained from Eq. (9) will be multiplied by 3 to enhance the contrast for displaying purposes [31].

3. The OCT system

In this study, we used a swept source OCT system with a swept source laser (SSOCT-1310, Axsun Technologies Inc., Billerica, MA). The laser has a central wavelength of 1310 nm, an A-line speed of 50 kHz and a total average power of 16 mW. The OCT system uses a Mach-Zehnder type interferometer with 90% of the light in the sample arm and 10% of the light in the reference arm. A dual-balanced detection scheme is used to acquire the signal. The system utilizes K-trigger mode. In the sample arm, a fiber collimator, a two-axis galvo mirror scanning system and an achromatic doublet with a focal length of 30mm are used. The collimator, galvo mirror scanner and the achromatic doublet are packaged in a handheld probe, achieving a beam diameter of 2 mm and a lateral resolution of 14.6 μm. For *in vivo* human imaging, the probe works in the contact mode so that the sample motion induced artifact is minimized.

4. Characteristics of the methods

4.1. Flow velocity determination

One of the attractive characteristics of PRCD is that quantitative information, such as the flow speed and direction can be measured when the probing beam is not in perpendicular to the flow. This characteristic of PRCD has been used for quantifying the flow rate, obtaining the flow profile, and analyzing the pulsation features of the flow [34–37]. However, the PRCD suffers from phase wrapping (or aliasing) and is strongly dependent on Doppler angle. The Doppler variance can also be used to quantify the flow speed with a pre-determined calibration curve when the probing beam is near perpendicular to the flow [33]. We have

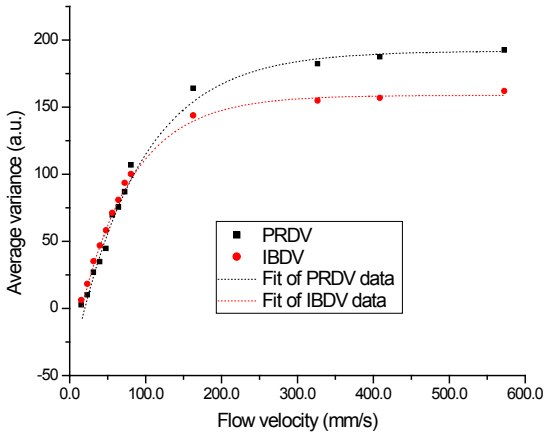

Fig. 1. The dependence of IBDV and PRDV values on the flow rate.

#172899 - $15.00 USD Received 19 Jul 2012; revised 11 Sep 2012; accepted 19 Sep 2012; published 26 Sep 2012

shown that IBDV is also able to quantify the flow speed with a pre-determined calibration curve [31]. Using PRCD to determine the flow velocity has been demonstrated by several groups [36,38]. Here, we compare the pre-determined calibration curves for PRDV and IBDV. The results are shown in Fig. 1. A flow phantom was used for obtaining these calibration curves. It is very interesting that the PRDV and IBDV show very similar features and both the curves are fitted well with exponential decay functions. At relatively lower speed regions, the curve shows a linear relationship between the flow speed and the variance values. At relatively higher flow speed regions, the curve shows saturation of the variance value.

4.2. Doppler angle dependence

PRCD values are sensitive to the Doppler angle [36]. In order to measure the absolute flow speed, we need to determine the Doppler angle. It has been found that PRDV is less sensitive to the Doppler angle when the probing beam is perpendicular to the flow [32]. We measured the Doppler variance as a function of the Doppler angle while keeping the flow speed constant. Our results here indicate that when the angular deviation from perpendicular incidence is small (below 12 degrees), the variance is independent of the Doppler angle. However, when the angular deviation from perpendicular incidence is relatively large (>12 degree), the Doppler variance is sensitive to the Doppler angle and the variance increases with the Doppler angle. The IBDV shows features similar to those of the PRDV (Fig. 2).

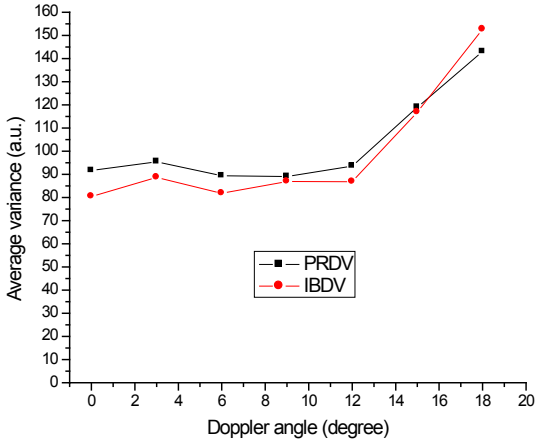

Fig. 2. The dependence of IBDV and PRDV values on the Doppler angle.

4.3. Velocity sensitivity improvement by increasing the time interval

According to Eq. (1), the adjacent phase difference [$d\theta(z)$] is proportional to the time difference (T) for a fixed Doppler frequency produced by the moving sample or moving particle in the sample. The phase difference can be "magnified" by the increasing time difference (T). This is a simple and effective way to improve the velocity sensitivity of the phase-resolved methods and has been adopted by several groups for ultrahigh sensitive imaging of blood vessels. We have demonstrated that increasing time difference (T) is also an effective way to improve the sensitivity of the IBDV method [31]. Here, with a flow phantom, we compared the effect of the time difference on the IBDV and PRDV values. A similar method as demonstrated in reference [31] was used to change the time interval. In brief, we acquired one frame of data with a very high sampling density level (ratio of beam spot size over A-line separations is about 134) and used part of the acquired data for processing to obtain results at different time intervals. The results are shown in Fig. 3. The characteristics of IBDV and PRDV are quite similar: the variance value increases proportionally with the increase of the time interval until the variance values reach saturation at large time intervals. One efficient way to obtain high velocity sensitivity is to apply the algorithms along the slow

#172899 - $15.00 USD Received 19 Jul 2012; revised 11 Sep 2012; accepted 19 Sep 2012; published 26 Sep 2012

scanning direction [8,12,16,20,30,31]. This inter-frame (IF) algorithm method can improve the velocity sensitivity without modification of the OCT hardware or software. We will use this inter-frame method in this manuscript.

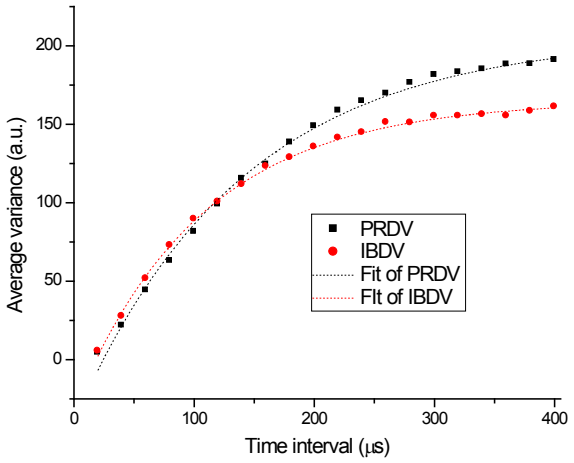

Fig. 3. The dependence of IBDV and PRDV values on the time interval.

5. *In vivo* mouse brain imaging

5.1. Animal preparation

To compare the performance of PRCD, PRDV and IBDV for the non-invasive imaging of microvasculature, we obtained transcranial OCT images of cerebrovascular circulation in mice. An adult 3-month old C57/BL6 male mouse was imaged. Imaging windows were created under gas mask isoflurane anesthesia (2% maintenance in 21% oxygen balanced by nitrogen) by removing the skin from bregma anteriorly to lambda posteriorly and bilaterally to the temporalis muscle attachments. The mouse skull was left intact and a saline-filled vasoline well covered by a glass coverslip was made as an imaging window. During the initial surgery and for the imaging session, the mouse was heated by a thermostatically-controlled heating pad (Gaymar). For imaging, isoflurane anesthesia was maintained at 1%. Excess gases were scavenged via a Bickford absorber unit and gas flow was maintained at 1.0 L/min. All procedures were performed in accordance with the regulations of the Institutional Animal Care and Use Committee (IACUC) of the University of California, Irvine.

5.2. Data processing

A traditional raster scanning protocol shown in Fig. 4 was used in this study. A total of 5120 frames with 1024 A-lines per frame were acquired. The whole 2D scan covered an area of 4 mm × 4 mm. All the images shown hereafter were processed off-line with custom software written with C++. During the data processing, the 3D data set (1024 by 5120 A-lines) saved on the hard disk was loaded into the computer memory and was re-saved on the disk as separate data files. Each separate data file contained 5120 A-lines with adjacent A-lines acquired along the slow scanning (Y) direction so that the algorithms are directly applied along the slow scanning direction without modification of existing processing software. There were a total of 1024 data files. The data process steps include spectrum averaging the background fringe, spectrum shaping with a Gaussian function and fast Fourier transform (FFT). The amplitude values of the complex analytical depth encoded signals were used to calculate the OCT images after logarithm calculation. The amplitude values of the complex analytical depth encoded signals were used to obtain the IBDV image, and the complex signals were used to obtain both the PRDV and PRCD images after bulk phase removal. For

#172899 - $15.00 USD Received 19 Jul 2012; revised 11 Sep 2012; accepted 19 Sep 2012; published 26 Sep 2012

the final PRDV, PRCD and IBDV images, an intensity threshold that was 5dB above the OCT intensity noise floor was used to eliminate the low scattering but high noise region. The *en face* IBDV images at different depths were extracted from the three dimensional IBDV tomographic images, and maximum intensity projection view *en face* images were processed from the *en face* IBDV images.

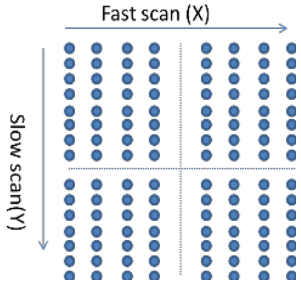

Fig. 4. Beam scanning protocol for acquiring the 3D OCT data set.

5.3. Results

Figure 5 shows the OCT images obtained by processing the data along the slowing scanning direction. Figure 5(c) shows the IF-PRCD image without bulk phase correction. Clearly, the phase changes between adjacent A-lines have a large random variation. We estimate that these random phase changes are due to bulk phase induced by the sample movement and the environment, such as vibration. This is quite different from the inter-A-line phase changes within a fast beam scanning frame, which usually is gradual. The effective time interval between the adjacent A-lines in the figures is 20 ms. For phase-resolved methods, the removal of bulk phase induced by bulk motion is necessary for high quality images. We have shown that Doppler variance is free from bulk motion induced artifacts when the bulk phase changes gradually [39]. For high resolution inter-frame methods used here, the change for bulk phase cannot be considered as gradually as shown in Fig. 5(b) and Fig. 5(c). Although some larger blood vessels as indicated by the red arrows can still be seen in the IF-PRDV image when carefully analyzing the image, the bulk phase greatly affects the image quality of both the IF-PRCD and the IF-PRDV images. Figure 5(d) shows the IF-IBDV image. It is evident that IF-IBDV is less sensitive to the miniature movement of the sample. Although there is no bulk motion correction procedure used for the IF-IBDV method, the vessels are clearly visible in the IF-IBDV image. Figures 5(e) and 6(f) are the IF-PRDV and IF-PRCD images with bulk

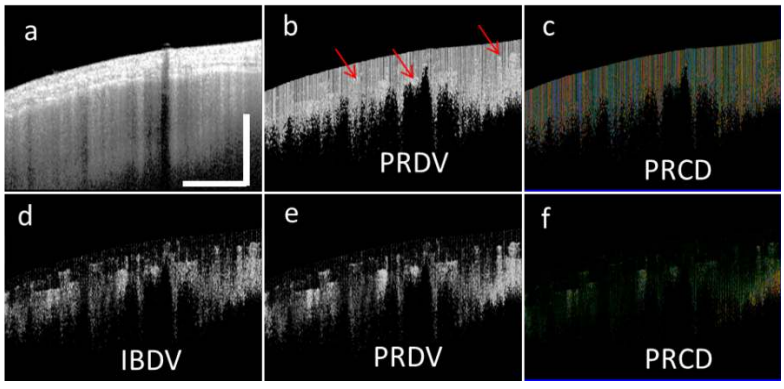

Fig. 5. *In vivo* OCT imaging of mouse brain with intact skull: (a) OCT image; (b) IF-PRDV image without bulk phase removal; (c) IF-PRCD image without bulk phase removal; (d) IF-IBDV image; (e) IF-PRDV image with bulk phase removal; (f) IF-PRCD image with bulk phase removal. Scale bar: 1mm.

#172899 - $15.00 USD Received 19 Jul 2012; revised 11 Sep 2012; accepted 19 Sep 2012; published 26 Sep 2012

phase corrected. The histogram based method is used to correct the bulk phase [39,40]. The method is effective for both IF-PRCD and IF-PRDV methods and the improvement can be clearly seen in Figs. 5(e) and 6(f). The bulk-phase corrected IF-PRDV image [Fig. 5(e)] is comparable to IF-IBDV image [Fig. 5(d)]. PRCD is able to differentiate the blood flow direction if the phase is not wrapped. However, the phase wrapped so significant in this case that it is not possible to tell the blood flow direction from the PRCD image. In the following paragraphs, the absolute value of the phase difference will be used for the PRCD image [10].

Usually, blood vessel networks are better viewed from an *en face* maximum intensity projection (MIP) view. Figure 6 shows the MIP view of IF-IBDV, IF-PRDV and IF-PRCD images. The depth information is color-coded in these images. The MIP view of IF-IBDV [Figs. 6(a) and 6(d)] and IF-PRDV images [Figs. 6(b) and 6(e)] are quite comparable to each other. Both of the variance methods are able to detect the capillary vessels with high sensitivity and high contrast. The IF-PRCD method shown in Figs. 6(c) and 6(f) is also sensitive for capillary vessels detection However, the contrast of the IF-PRDV and IF-IBDV methods, is better than that of IF-PRCD image, especially in the regions with smaller blood vessels.

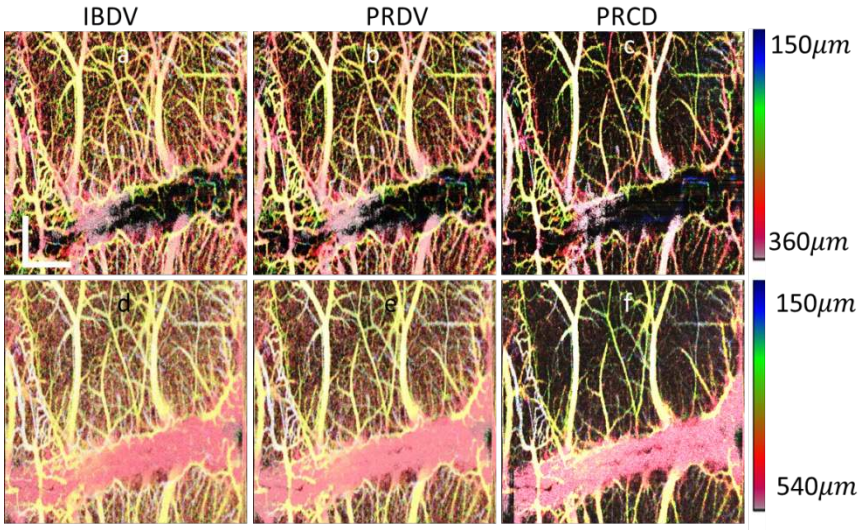

Fig. 6. *En face* maximum intensity projection (MIP) view image of mouse brain with intact skull. (a) MIP view IF-IBDV image for depth 0–360 μm. (b) MIP view IF-PRDV image for depth 150–360 μm. (c) MIP view IF-PRCD image for depth 150–360 μm. (d) MIP view IF-IBDV image for depth 150–540 μm. (e) MIP view IF-PRDV image for depth 150–540 μm. (f) MIP view IF-PRCD image for depth 150–540 μm. Scale bar, 1mm.

6. *In vivo* human skin imaging

For *in vivo* awake human imaging, the involuntary movement of the subject usually induces bulk motion artifacts which will affect the image quality. To reduce this effect, we used a handheld imaging probe which worked in a contact mode for human skin imaging. Figure 7 shows the results of OCT images for human palm skin. Figure 7(a) shows the photogram of the imaged region. Figures 7(b)–7(j) shows the *en face* MIP images. In the superficial regions (120–360 μm), the capillary loops, which show up as bright dots in the *en face* MIP view images, are clearly visible [Figs. 7(b)–7(d)]. With an increase of the depth, several miniature vessel branches are also clear in the images [Figs. 7(e)–7(g)]. The vessel diameter increases in the deeper regions [Figs. 7(h)–7(j)]. The results match well with the skin vasculature anatomy, which shows small capillary loops coming up from the deeper layer of arterials and venules. There are a few horizontal lines in both the IF-PRDV and IF-PRCD images as indicated by

#172899 - $15.00 USD Received 19 Jul 2012; revised 11 Sep 2012; accepted 19 Sep 2012; published 26 Sep 2012

the arrows [Figs. 7(c), 7(d), 7(f), 7(g), and 7(j)]. However, these horizontal lines are not shown in the IF-IBDV images. This demonstrates that the IBDV method is less sensitive to the sample bulk motion and the phase-resolved methods are more vulnerable to motion artifacts. The other findings are similar to those from previous mouse brain results: the IF-IBDV and IF-PRDV images are comparable to each other and the PRCD images show lower contrast. The IBDV method benefits from an easy processing procedure compared with phase-resolved methods which require phase stability improvement and removal of bulk motion induced bulk phase.

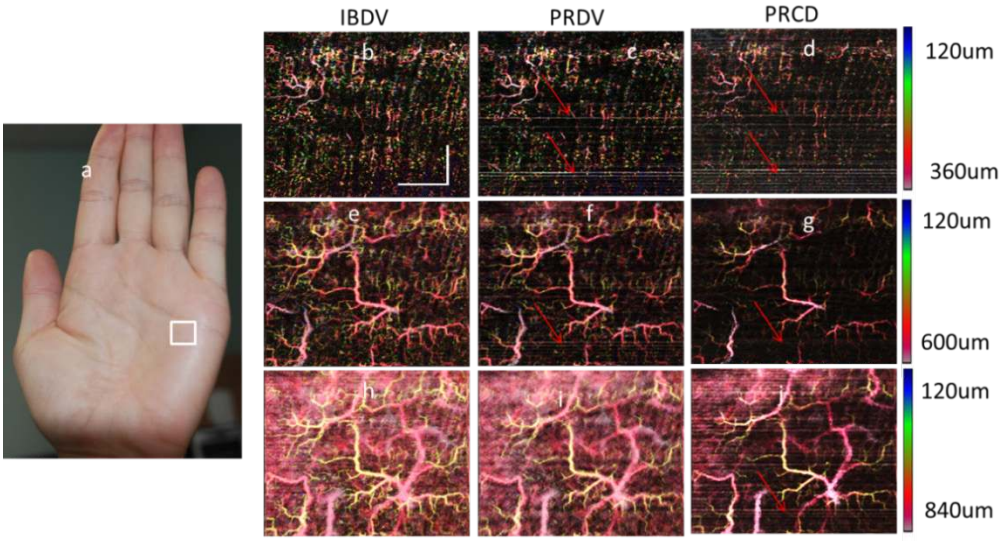

Fig. 7. *En face* MIP view image of human palm skin. (a) Photography of the imaging area (in the white rectangle). (b) *En face* MIP view IF-IBDV image for depth of 120–360 μm. (c) En face MIP view IF-PRDV image for depth of 120–360 μm. (d) *En face* MIP view IF-PRCD image for depth of 120–360 μm. (e) *En face* MIP view IF-IBDV image for depth of 120–600 μm. (f) *En face* MIP view IF-PRDV image for depth of 120–600 μm. (g) *En face* MIP view IF-PRCD image for depth of 120–600 μm. (h) *En face* MIP view IF-IBDV image for depth of 120–640 μm. (i) *En face* MIP view IF-PRDV image for depth of 120–840 μm. (j) *En face* MIP view IF-PRCD image for depth of 120–840 μm. Scale bar, 1mm.

7. Summary

In summary, we compared in detail three methods which use, respectively, phase information, intensity information, and both phase and intensity information. A flow phantom was used to obtain the performance parameters of these methods. These parameters included the flow speed determination, incident angle dependence, and sensitivity improvement by increasing the adjacent A-line time intervals. It was found that all the methods were able to quantify the flow speed when the flow rate is within a certain range which is related to the adjacent A-line time interval. While PRCD is most sensitive when the flow direction is along the probing beam, PRDV and IBDV are better to measure the flow when the flow direction is near perpendicular to the probing beam. The PRDV and IBDV were not sensitive to the Doppler angle when the angular deviation from perpendicular incidence was less than 12 degrees. However, the PRDV and IBDV were Doppler angle-dependent when the angular deviation from perpendicular incidence was larger than 12 degrees. The sensitivity of all the methods could be improved by increasing the time interval while still maintaining a high sampling density level. *In vivo* imaging of mouse brain with intact skull and human palm skin were demonstrated. The vascular network images obtained with the three methods were compared, and the IBDV method was found to be able to obtain high resolution image with a relative simple processing procedure.

#172899 - $15.00 USD Received 19 Jul 2012; revised 11 Sep 2012; accepted 19 Sep 2012; published 26 Sep 2012

Acknowledgments

This work was supported by the National Institutes of Health (R01EB-10090, R01HL-105215, R01HL-103764, R01EY-021529 and P41EB015890), Air Force Office of Scientific Research (FA9550-04-0101), and the Arnold and Mabel Beckman Foundation. Dr. Chen has a financial interest in OCT Medical Imaging Inc. which, however, did not support this work.

#172899 - $15.00 USD Received 19 Jul 2012; revised 11 Sep 2012; accepted 19 Sep 2012; published 26 Sep 2012